Collective Electronic Oscillators for Second-Order Polarizabilities of Push−Pull Carotenoids†

Timothée Toury,‡,§ Joseph Zyss,*,§ Vladimir Chernyak,‡ and Shaul Mukamel*,‡

Department of Chemistry, University of Rochester, Rochester, New York, 14627, and Laboratoire de Photonique Quantique et Moléculaire et Département de Physique, Ecole Normale Supérieure de Cachan, 61 avenue du Président Wilson, 94235 Cachan, France

The first off-resonance hyperpolarizabilities ($\beta(0)$) of bisubstituted carotenoids are computed and analyzed using a quasiparticle, collective electronic oscillators (CEO) representation. The few oscillators which dominate the response are identified by solving the time dependent Hartree−Fock equations for the reduced single electron density matrix. The variations of these oscillators and the relevant anharmonicities with bridge length are studied. The present approach does not suffer from the difficulties which prevent the development of a simple intuitive picture in the commonly used sum-over-states expressions (i.e., strong interference effects and unphysical size scaling of various contributions). Displaying the CEO in real space provides an intuitive picture of the origin of the nonlinear response and the scaling and saturation of $\beta(0)$ for large sizes.

I. Critical Survey of Quantum Computational Techniques in Molecular Engineering

The design of new molecules with large optical nonlinearities is crucial for a broad range of applications to optical signal processing and telecommunication.[1−3]

Practical implementation and success of a molecular engineering approach rests on the reduction of an abundance of structural and spectroscopic features down to a limited number of parameters. These must embody the essence of the mechanisms underlying the optical phenomena of interest and should furthermore be amenable to chemical intuition so as to provide practical guidelines toward synthesis and subsequent efficiency optimization. A priori complex computational methods are then amenable to much simpler tractable and insightful models.

As most obvious examples of such comprehensive features, symmetry related considerations have been shown throughout the development of this field to play a basic role. In the case of the quadratic process, the well-known constraint of departure from centro-symmetry provides a stringent prerequisite all the way to the more elaborate 2-D and 3-D multipolar symmetry considerations currently under investigation.[4−6] Such considerations have indeed highlighted the role of multiple charge transfer and the importance of the relative positions of the various donor and acceptor groups as well as that of the polarizable connecting moieties between such groups. The paradigm in the domain of quadratic molecular nonlinear optics is thus currently shifting from the rodlike paranitroaniline dipolar template to a cube or more generally a rhombohedron with alternating donor and acceptor functional groups at the corners and center abiding to tetrahedral geometry, of which the earlier pNA template appears to be a specific case.[4,7] Whereas such powerful symmetry-related features have indeed provided stringent guidelines, they still fall short of providing quantitative information as to the magnitude of phenomena very much like selection rules in spectroscopy are operational to determine the allowance of a transition but fail to account for its strength.

It is the purpose of this work to apply the *collective electronic oscillators* (CEO) framework toward the evaluation and interpretation of hyperpolarizabilities.[8−10] The classical anharmonic oscillator picture proposed by Bloembergen[11] stands-out as an early attempt in this direction based on the extension of the Lorentz−Lorenz harmonic oscillator approach of linear properties[12] which has served throughout almost four decades of nonlinear optical material research as a useful guideline. It was precisely the deviation of many organic materials from Miller δ which had pointed-out the interest of molecular materials for such applications.[13,14] δ is defined as the ratio of the $\chi^{(2)}$ quadratic susceptibility of a given material over a cubic product of its linear $\chi^{(1)}$ susceptibilities at ω and 2ω. Whereas its magnitude does not deviate by more than a factor of 2 from an average value of 2×10^9 for inorganic materials, it can surpass this standard average by as much as 2 orders of magnitude in organic molecule based compounds. This deviation is an indication of a much higher inelastic constant for organics than for inorganics in the anharmonic oscillator picture for electronic susceptibilities. This model is based on the assumed existence of a classical anharmonic restoring potential experienced by electrons as they are driven out of mechanical equilibrium by an external field. Within this model, polarizabilities of arbitrary orders can be connected to derivatives of the potential of the same order taken at mechanical equilibrium which then serve as empirical parameters. Within this picture, the second order derivatives lead to three basic linear oscillator frequencies which appear in frequency dependent resonant denominators. This somewhat empirical model does not reflect the basically quantum nature of light-matter interactions at the molecular level and cannot be expected to provide more than basic trends and order of magnitude agreements. The model has often been used for qualitative back of the envelope estimates but was not considered a rigorous approach with quantitative value.

The CEO approach retains the simplicity of the anharmonic picture while providing a more relevant quantum picture of photoinduced electronic displacements in terms of a restricted

† Part of the special issue "Edward W. Schlag Festschrift".
* To whom correspondence should be addressed.
‡ University of Rochester.
§ Ecole Normale Supérieure de Cachan.

10.1021/jp004471j CCC: $20.00
Published on Web 05/22/2001

number of quantized electron oscillators. Moreover, these are not a priori or empirically given as in the earlier classical anharmonic picture but derived from the full Hamiltonian of the light-molecule system. Our primary goal in this study is to explore the possibility of extracting from the full set of electronic anharmonic oscillator solutions of the Liouville equation driving the density matrix of the molecular system under coherent illumination, a limited number of such oscillators capable of accounting with reasonable accuracy for the overall nonlinear quadratic susceptibility; we further attach inasmuch as possible chemically intuitive significance to these relevant oscillator modes for a given series of molecules deriving from a common pattern.

Several other approaches are commonly applied toward the quantitative estimation of nonlinear optical susceptibilities. One of the most commonly used is the sum-over-state formalism[15−17] derived from Ward's perturbative expression.[18] It was however more successful in accounting for the experimentally determined magnitudes of susceptibilities than in providing instrumental guidelines for molecular engineering. This is due to the highly numerical nature of this approach whereby precision is attached to the dimension of the Hilbert space of representation and to the number of singly and eventually multiply excited configurations participating in the expansion. A quantitative analysis aiming at identifying those states which significantly contribute to the full perturbation expansion has been proposed and applied to the quadratic and cubic polarizabilities of standard charge transfer in aromatic molecules.[19,20] Various rational ways to condense the information have been proposed in order to single out and extract possibly dominant excited-state contributions to such an expansion so as to be able to eventually relate these to dominant molecular features. In view of the empirical evidence of the crucial role played by charge transfer in quadratic optical polarizabilities as well as of the occurrence of a clear linear spectroscopic signature of donor−acceptor charge transfer in the form of a dominant charge-transfer band in the UV−visible absorption spectrum of the species of interest, it was naturally proposed at an early stage to model the pNA template as well as related rodlike dipolar donor−acceptor conjugated structures by a two-level system. This approach has been implemented by way of extending to nonlinear optics Mulliken's classical approach of linear properties[21,22] in terms of two or three resonant mesomeric structures, namely, the neutral state ($D \leftrightarrow A$), the direct ($D^+ \rightarrow A^-$), and eventually the inverse ($D^- \leftarrow A^+$) mesomeric representations of the molecule. It is then a simple matter to evaluate higher order molecular polarizabilities within such a two-state picture leading to a (2×2) Hamiltonian with two eigenstates meant to embody within a so-called "two-level model" essential properties of the ground and charge transfer states as well as their contribution to the quadratic polarizabilities.[23−26]

To fit experimental data into this model and check its validity, $\boldsymbol{\mu}_{01}$, the transition dipole of the charge transfer excitation (or equivalently its oscillator strength) and $\Delta\boldsymbol{\mu} \equiv \boldsymbol{\mu}_{11} - \boldsymbol{\mu}_{00}$, the difference between ground and excited-state dipole moments, can be inferred indirectly from the experimental values of the linear and quadratic polarizabilities α and β as modeled within the two-state frame. Alternatively, they can be obtained more directly from a rich and purposely redundant combination of experiments such as real and imaginary linear index measurements in solution and solids by spectroscopic ellipsometry,[27] linear absorption spectroscopy, solvatochromism,[28] measurement of the ground-state dipole moment such as the Guggenheim capacitive method,[29−31] or electroabsorption.[32,33] β can be extracted from electric field induced second-harmonic generation measurements[34−36] which, under poling of molecules by an externally applied voltage, provide the projection of the vector part of β on the ground-state dipole $\boldsymbol{\mu}_{00}$. An alternative more recent technique uses the more versatile harmonic light scattering[37−41] which provides more tensorial information than the former because of its less symmetry-constrained configuration thanks to the absence of an electric poling field. Validity of the model can then be checked by comparison of the $\boldsymbol{\mu}_{01}$ and $\Delta\boldsymbol{\mu}$ values resulting from application of the two-level expressions to the experimental α and β values with those directly inferred from the arsenal of complementary spectroscopic and dielectric experiments as listed above. Results are generally satisfactory in situations whereby the upper harmonic photon energy $2\hbar\omega$ is close enough to the absorption band so that other potentially contributing excited states can then be safely ignored. It is however necessary to introduce further line broadening mechanisms (e.g., excited-state lifetimes and pure dephasing) to account for the resonant or quasiresonant nature of the excited-state population process.[42,43] The limitations of such an approach have been recognized at an early stage in the context of cubic nonlinear processes where contributions to the cubic hyperpolarizability γ of four-photon Ward diagrams connecting the lower lying excited state to higher lying ones play an important and sometimes dominant role.[44,45]

Moreover, and still in the realm of quadratic nonlinearities, it was shown[46−48] on the basis of joint spectroscopic and symmetry considerations that a minimum of three levels are needed to account for the quadratic nonlinearity of octupoles due to the intrinsic 2-fold degeneracy associated with the irreducible representations of the typical E (or E') labeled excited states participating in the 3-fold symmetry octupolar charge-transfer process. A formal link between the minimal dimensionality of the excited-state Hilbert representation on the one hand and the rank of the physical tensorial property of interest (e.g., 3 for tensor β) can be found in ref 48. Proposition of other "minimal basis states" strategies have been inspired by the development of multipolar charge-transfer candidate molecules based on a generalized Mulliken scheme involving a neutral valence band state connected to a series of charge transfer states according to the multiple substitution pattern of the 2-D and 3-D multipolar molecule.[49,50] In particular, β properties of 2-D 3-fold symmetry octupoles have been shown to satisfactorily abide respectively to a four states (VB-3CT model Hamiltonian based on the three charge-transfer excited states along the three blades of the trigonal octupole and the neutral "valence band" ground state). β properties of 3-D tetrahedral octupoles[51] were described using a five state (VB-5CT model with four charge-transfer excited states along the four directions from the center of a tetrahedron to its ends plus the neutral valence band ground state). In the realm of inorganic solids, both dieletric and semiconducting, the Philips and Van Vechten model[52] such as applied to chalcopyrites and other classes of oxyde crystals[13] and semiconductors[14,53] is based on the utilization of a reduced number of structural bonding features such as ionicities and electron affinities or overlap factors of the connected atoms. This approach has been successful in outlining an optimal combination of donor and acceptor atoms to enhance $\chi^{(2)}$ for mineral solids leading to similar trends as were proposed later in the context of molecules.[54]

This approach is particularly useful for the near resonant response but becomes tedious in the off-resonance regime where many eigenstates contribute. A few-level model which artificially removes most eigenstates involved in the nonlinear

response is commonly used. Although different variants of this approach have proved somehow useful within the reduction scheme aiming at the identification of a limited set of parameters believed to play a significant role in optical processes at the molecular level, their limited validity, mainly restricted to the field of resonant processes, therefore falls short of providing a dispersion free guideline that would also apply to the nonresonant parametric regime whereby purely virtual transitions are participating. A typical approach which may be applicable to off-resonant conditions, however, not to resonant ones, is based on Unsöld approximation,[55−57] which consists of averaging the "details" of individual excited states by reducing their full manifold into a single equivalent excited state, the practical condensation being dictated by the f-sum rule. It has been shown in this context that nonlinearities can be connected to multipolar moments of the ground-state charge density with, for example, α proportional to the quadrupolar and β to the octupolar moment. Recent testing of this approach on the basis of experimental charge density determinations from X-ray diffraction studies in single crystals have however pointed out the limitations of this approach even in the nonresonant regime where it should be in principle applicable.[58]

A totally different approach, known as the finite-field method, has been applied early on[59] to the evaluation of static (e.g., zero frequency) hyperpolarizabilities of charge transfer systems and is being routinely implemented in quantum computer packages. Rather than using a perturbative treatment à la Ward, it is based on the direct computation (e.g., iterative diagonalization) of a full self-consistent Hamiltonian accounting for the electronic systems and nuclei, which includes a dipolar coupling energy term $W = -\boldsymbol{\mu}\cdot\boldsymbol{E}$. It therefore allows us to evaluate all field-dependent observable quantities, including the induced dipole $\boldsymbol{\mu}(\boldsymbol{E})$ or the field-dependent energy. The accuracy of this evaluation depends critically on the numerical precision of the diagonalization procedure as well as on the dimension and nature of the atomic orbital space sustaining the molecular orbital wave function Hilbert space within a Roothan−Hartree−Fock picture. Differentiation of the three components of the induced dipole or of the field-dependent energy with respect to the comparatively weak applied polarizing $\boldsymbol{E}$ field components leads, in a Cartesian framework, to the tensorial coefficients of hyperpolarizabilities of successive orders (this is best approximated by considering differences of the induced dipole under symmetrical finite field steps of different small magnitudes). This method solely focuses on ground-state wave functions and therefore does not incorporate explicitly dipolar transitions between various states, contrary to the perturbative sum over states approach whereby excited states and their couplings are the basic ingredients. This method is not designed to help identify those excited states which contribute significantly to the nonlinearity of interest. It is nevertheless well tailored for estimating the magnitudes of static polarizabilities, in contrast with methods based on a reduced number of excited states which are likely to provide better results at the vicinity of a transition.

The CEO formalism used here provides a more general approach which is applicable with equal relevance far from resonance as well as in quasiresonant configurations, and its application would be of major interest in particular in order to account for both nonresonant electrooptic effects and the corresponding quasiresonant case of second-harmonic generation. Indeed, applications of electrooptic polymers are mostly in demand at high bandwidth operation conditions as driven by an off-resonant molecular polarizability $\beta_{EO}(-\omega - \Omega;\omega,\Omega)$ with ω corresponding to the infrared carrier wavelength in the 1.55 μm window of silica fibers and Ω in the tens of GHz microwave bandwidth,[60] whereas typical charge-transfer resonances, in the 500−600 nm range for nonlinear chromophores tethered to a transparent polymer backbone, stand far above the infrared carrier photon energy. Preliminary to electrooptic measurements which required a somewhat involved permanent poling procedure, it is customary to scan candidate molecules via a second-harmonic generation experiment in solution which leads to the $\beta_{SHG}(-2\omega;\omega,\omega)$ tensor. In sharp contrast with β_{EO}, the β_{SHG} tensor is quasiresonant as the 2ω frequency comes more closely to the onset of absorption than in the electrooptic case. Regardless of other deeper fundamental reasons, the need for a single framework capable of consistently accounting for both resonant and off-resonant regimes appears thus particularly striking in order to be able to match the needs of current experimental methodology in the realm of electrooptic molecular engineering.

II. Electronic Oscillators and Molecular Polarizabilities in the CEO Framework

Assuming a two-level model, the two lowest order off-resonance polarizabilities have the following form:

$$\alpha(0) \propto \frac{\boldsymbol{\mu}_{ge}^{\,2}}{\omega_{ge}}; \quad \beta(0) \propto \frac{(\boldsymbol{\mu}_{ee} - \boldsymbol{\mu}_{gg})\boldsymbol{\mu}_{ge}^{\,2}}{\omega_{ge}^{\,2}} \tag{1}$$

$\boldsymbol{\mu}_{ee}$ and $\boldsymbol{\mu}_{gg}$ are respectively the permanent dipole moments of the ground ($|g>$) and the excited ($|e>$) states, $\boldsymbol{\mu}_{ge}$ is the transition dipole moment between these two states, and ω_{ge} is the transition frequency.[1,61] Considering a family of donor−bridge−acceptor molecules, $\beta(0)$ has two factors with opposite scaling as the length of the bridge (the number of double bonds, N) is increased: $\boldsymbol{\mu}_{ge}^{\,2}/\omega_{ge}^{\,2}$ grows $\sim N$, whereas $(\boldsymbol{\mu}_{ee} - \boldsymbol{\mu}_{gg}) \sim 1/N$. This canceling of a diverging and vanishing factors prevents an easy intuitive prediction of the evolution of the properties with N, making it especially difficult to predict and rationalize the saturation of $\beta(0)$ for large bridge lengths. Moreover, retaining only few levels may not be justified theoretically in the off-resonant regime.

The oscillator (*quasiparticle*) picture used in this article has numerous conceptual and numerical advantages over the eigenstate representation[8,65] and automatically cures the difficulties outlined above. Rather than considering a basis set of eigenstates of the Hamiltonian to represent the *wave function*, we use a basis of CEO to represent the *reduced one electron density matrix*.[8,63−66] In contrast with the eigenstate representation, it has been shown that only a limited number of these oscillators are involved in the response. We thus obtain a simple, classical, yet fully microscopic picture of the nonlinear optical process. The few-oscillator model provides an alternative to the few-level model. By displaying the oscillators in the atomic basis set, we obtain a highly intuitive picture of the behavior of the molecule during the course of the nonlinear optical response. The relevant regions of the molecule and their couplings and coherences are clearly identified, resulting in a global picture of the dynamics of optical excitations in terms of a set of interacting functional groups. The degree of involvement of various regions can be visualized, resulting in a new, deeper, and highly intuitive approach for the design of optical materials.

The CEO approach starts with the reduced single-electron ground-state density matrix,[69,70] defined as

$$\bar{\rho}_{nm} \equiv \langle \psi_g | c_n^+ c_m | \psi_g \rangle \tag{2}$$

where c_n^+ and c_m are respectively the Fermi creation and

annihilation operators (spin indices have been omitted for brevity). ψ_g is the many electron ground-state wave function. The *n*th diagonal element of this matrix (*population*) represents the charge of the *n*th orbital, whereas the off-diagonal element $\bar{\rho}_{nm}$ (*coherence*) is a measure of the chemical bond strength between atoms *n* and *m*.[62,71,72]

When the molecule is subjected to a time-dependent electromagnetic field, its density matrix becomes time-dependent as well:

$$\rho_{nm}(t) \equiv \langle \psi_g(t)|c_n^+ c_m|\psi_g(t)\rangle \tag{3}$$

We then have

$$\rho(t) = \bar{\rho} + \delta\rho(t) \tag{4}$$

Separating the hole-particle (ξ) and particle−particle/hole−hole ($T(\xi)$) contributions to $\delta\rho$, we obtain

$$\rho(t) = \bar{\rho} + \xi(t) + T(\xi(t)) \tag{5}$$

The density matrix corresponding to a single Slater determinant is idempotent:

$$\rho(t) = \rho^2(t) \tag{6}$$

It immediately follows from eqs 5 and 6 that $T(\xi(t))$ can be expressed in terms of $\xi(t)$:

$$T(\xi) = (I/2 - \bar{\rho})\cdot(I - \sqrt{I - 4\xi^2}) \tag{7}$$

I being the unit matrix.

The oscillator variables are the eigenmodes of the linear part of the time-dependent Hartree−Fock equations (where the terms with $(\delta\rho)^2$are not retained):

$$L|\xi_\alpha\rangle\rangle = \Omega_\alpha|\xi_\alpha\rangle\rangle \quad \text{and } L|\xi_{-\alpha}\rangle\rangle = -\Omega_\alpha|\xi_{-\alpha}\rangle\rangle \tag{8}$$

with the normalization

$$\langle\langle\xi_{-\alpha}|\xi_\alpha\rangle\rangle \equiv Tr(\bar{\rho}[\xi_{-\alpha}, \xi_\alpha]) = 1 \tag{9}$$

The electron−hole part of the density matrix can be expanded as

$$\xi(t) = \sum_{\alpha>0}[\xi_\alpha z_\alpha(t) + \xi_\alpha^+ z_\alpha^*(t)] \tag{10}$$

The oscillator amplitudes come in complex conjugate pairs z_α and z_α^* and satisfy the relations $\xi_{-\alpha} = \xi_\alpha^+$ and $z_{-\alpha} = z_\alpha^*$. Here, ξ_α is an oscillator described by the two operator ξ_α and ξ_α^+. These operators may be combined to form real operators that represent the oscillator coordinates and momenta:

$$\hat{Q}_\alpha = \frac{1}{\sqrt{2}}(\xi_\alpha + \xi_\alpha^+); \quad \hat{P}_\alpha = \frac{i}{\sqrt{2}}(\xi_\alpha - \xi_\alpha^+) \tag{11}$$

The electronic excitations are now described as classical anharmonic oscillators with amplitudes z_α. Using a basis set with N_h occupied and N_p unoccupied molecular orbitals, there are $N_p\cdot N_h$ oscillators which come in pairs and satisfy the following equations of motion:[67,68]

$$i\frac{\partial}{\partial t} z_\alpha = \Omega_\alpha z_\alpha - \epsilon(t)\cdot\boldsymbol{\mu}_\alpha - \epsilon(t)\cdot\sum_\beta \boldsymbol{\mu}_{\alpha,\beta} z_\beta + \sum_{\beta\gamma} V_{\alpha,\beta\gamma} z_\beta z_\gamma \tag{12}$$

where Ω_α is the oscillator frequency, $V_{\alpha,\beta\gamma}$ are the anharmonicities, and $\boldsymbol{\mu}_\alpha$ and $\boldsymbol{\mu}_{\alpha,\beta}$ are dipole moments. These classical equations may be rigorously derived from the quantum molecular Hamiltonian, as shown in Appendix A.

The polarization (the expectation value of the dipole operator) which is responsible for all optical signals is given by

$$\mathbf{P} = \sum_\beta \boldsymbol{\mu}_\beta z_\beta + \sum_{\beta,\gamma} \bar{\boldsymbol{\mu}}_{\beta,\gamma} z_\beta z_\gamma \tag{13}$$

where $\bar{\boldsymbol{\mu}}_{\beta,\gamma}$ defined in eq B11 represents the nonlinear dependence of the dipole on oscillator coordinates. All parameters of eqs 12 and 13 may be obtained from the fully microscopic Hamiltonian, as shown in Appendix A. Equations 12 and 13 generally have higher order terms (products of more *z* factors), but they may be rigorously truncated for the sake of computing low order polarizabilities. The present truncation is sufficient for computing $\beta(0)$.

Equation 12 can be solved order by order in the external field $\epsilon(t)$, resulting in the optical response functions. For the linear response, we have (the superscript denotes the order in the field)

$$\mathbf{P}^{(1)} = \sum_\beta \boldsymbol{\mu}_\beta z_\beta^{(1)} \tag{14}$$

which gives for the static linear polarizability

$$\alpha(0) = \sum_\beta \frac{\boldsymbol{\mu}_\beta \boldsymbol{\mu}_\beta}{\Omega_\beta} \tag{15}$$

The second-order response is given by

$$\mathbf{P}^{(2)} = 2\sum_\beta \boldsymbol{\mu}_\beta z_\beta^{(2)} + \sum_{\beta,\gamma} \bar{\boldsymbol{\mu}}_{\beta,\gamma} z_\beta^{(1)} z_\gamma^{(1)} \tag{16}$$

which yields

$$\beta(0) = -2\sum_{\alpha\beta\gamma} U_{\alpha,\beta\gamma} \frac{\boldsymbol{\mu}_\alpha \boldsymbol{\mu}_\beta \boldsymbol{\mu}_\gamma}{\Omega_\alpha \Omega_\beta \Omega_\gamma} + 3\sum_{\beta\gamma} \frac{\boldsymbol{\mu}_\beta \bar{\boldsymbol{\mu}}_{\beta,\gamma} \boldsymbol{\mu}_\gamma}{\Omega_\beta \Omega_\gamma} \tag{17}$$

where $U_{\alpha,\beta\gamma}$ is defined in eq B10. The summations in eqs 14−17 run over positive values of the indices.

Equation 17 employs the complete basis set of spin−orbitals. If the electrons are counted in pairs, a factor 2 must be added in this formula. This point should become clear in the following section and the appendix. Moreover, when computing off-diagonal components of the $\beta(0)$ tensor, eq 17 must be symmetrized over the tensorial components of the incoming field. Adopting a tensor notation $\beta(0)_{i,jk}$, $\epsilon_j \otimes \epsilon_k$ is the incoming field and ϵ_i is the outgoing field.

III. Application to Push−Pull Carotenoids

We have studied the variation of the electronic oscillators with bridge length for a series of bisubstituted carotenoids (CAR(*j*)) with a dimethylamine donor and a two cyano group for the acceptor (Figure 1). The bridge length (*j*) was varied from 2 to 25 double bonds. This system was chosen because it is typical of polyenic oligomers used in electroluminescent devices,[73] and numerous measurements have been made on these and similar molecules.[74−76]

We have considered carotenoids without methyl groups on the bridge. These groups do not affect $\beta(0)$ by more than 10%, and for the most part, their effect is primarily steric rather than inductive. Geometry optimization was done at the semiempirical

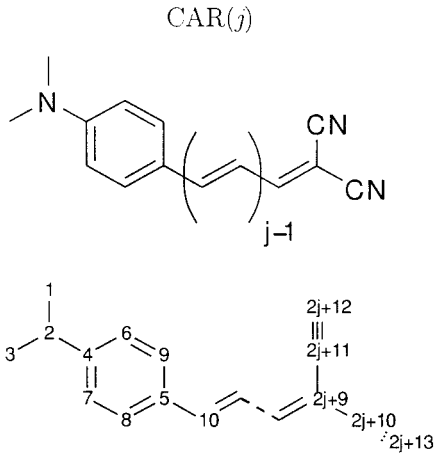

Figure 1. Structure and atom labeling of the bisubstituted carotenoid with a j double bonds bridge CAR(j). The atom labels $n = 1...2j + 13$ are shown in the lower structure.

AM1 level using Gaussian 98.[77] Intramolecular charge transfer is very sensitive to the conformation; thus, to better demonstrate general trends, the aromatic ring and the polyene bridge were constrained to be planar. The optimization was made to mimic the chromophore geometry in the material (by choosing the geometry optimization method and the constraint) even though the computation is performed for the isolated molecule. The molecules are oriented along the $\overrightarrow{Ox}$ axis, and hereafter, we only consider the most important component ($\beta_{xxx}(0)$) of the $\beta(0)$ tensor.

The INDO/S Hamiltonian[78−80] and the dipole operator were computed in the atomic basis set using the ZINDO code. Each hydrogen is assigned a single s basis function, whereas carbons and heteroatoms have 1 s and 3 p atomic orbitals. Because we consider closed shell configurations, spin variables may be eliminated and the electrons are counted in pairs. The Hartree−Fock approximation is used to compute the ground-state reduced single electron density matrix $\bar{\rho}_{nm}$. Then the first 50 eigenmodes of eq 8 are computed with the oblique Lanczos algorithm.[81] Several convergence tests were made for the number of modes and the precision parameters required by the iterative methods. $\beta(0)$ varied by less than 5% between these tests.

The eigenmodes were then ranked according to the magnitude of $\boldsymbol{\mu}_\alpha/\Omega_\alpha$ and only the first 20 oscillators were retained. All of the necessary quantities for the calculation of $\beta(0)$ are obtained, and $\beta(0)$ is then computed using the first 1−20 oscillators. This reveals the degree of involvement of each oscillator in the second-order response. Figure 2 displays $(\beta_{k-1}(0) - \beta_k(0))$ versus k, where $\beta_k(0)$ is $\beta(0)$ computed with the first k oscillators. This figure shows the contribution of each additional oscillator to CAR(9). Other sizes up to CAR(17) show a very similar pattern (not shown). The ordering of the oscillators (by $\boldsymbol{\mu}_\alpha/\Omega_\alpha$) does not affect the contribution of each oscillator.

It is remarkable that only two oscillators are dominant for this series of carotenoids and are responsible for 70−90% of $\beta(0)$. The contribution of the second oscillator always has opposite sign to the first. Hereafter, we denote the first oscillator $\xi+$ and the second $\xi-$. We have therefore computed the first off-resonance hyperpolarizability using these two oscillators. The variation of $|V_{\alpha,\beta\gamma}|$ and $|\boldsymbol{\mu}_{\alpha\beta}|$ with the bridge length is displayed in Figure 3 and given in Table 1. We note that very few anharmonicities and coupling coefficients are dominant.

The variation of $\beta(0)$ with bridge length is displayed in Figure 4. The lower panel shows the second term of eq 17, representing

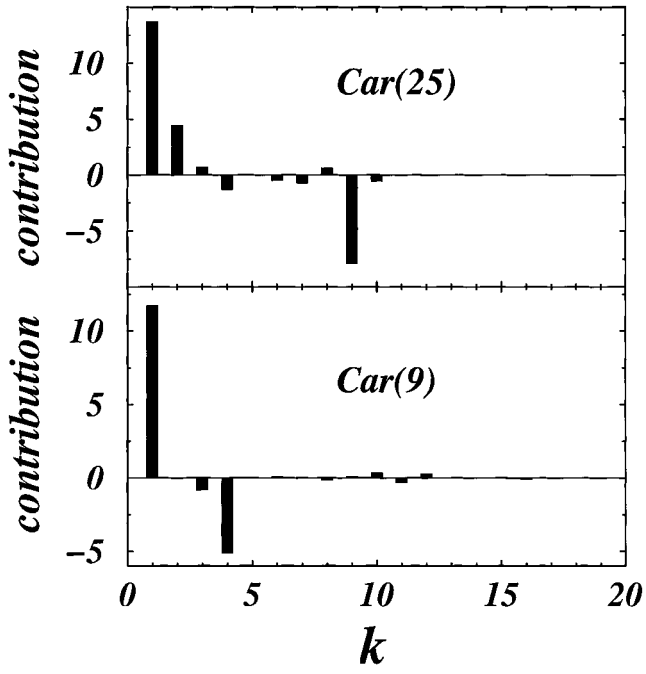

Figure 2. Contribution of the kth oscillator to $\beta(0)$ (e Å^3 V^{-2}) for CAR(9) and CAR(25).

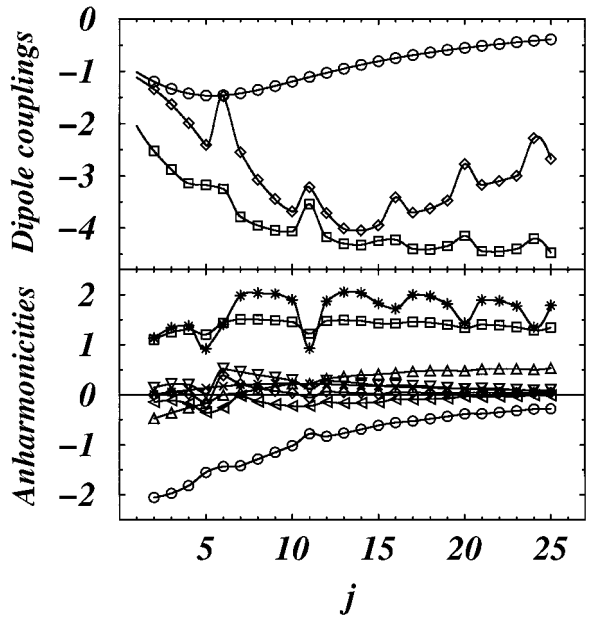

Figure 3. Variation of the anharmonicities (e V) and dipole coupling coefficients (e Å) with the number of double bonds (the various contributions may be identified using Table 1).

the contribution of the coupling dipole $\boldsymbol{\mu}_{\alpha\beta}$ to $\beta(0)$ (△), the first term coming from the anharmonicities (◇) and the total $\beta(0)$ for the two-oscillator model (○). In the upper panel, $\beta(0)$ obtained from the two-oscillator model (□) is compared to the full CEO calculation involving all 50 oscillators (○). For bridge lengths up to 11 double bonds, the two-oscillator model provides an adequate description. Both contributions to $\beta(0)$ saturate at about 14 double bonds.

Figure 5 depicts the ground-state density matrix (top row) and the oscillators $\xi+$ (middle row) and $\xi-$ (bottom row) for CAR(3) (left column), CAR(7) (middle column), and CAR(25) (right column). They are represented in real space using the atomic basis set (the coordinates show the atom number as given

TABLE 1: Coupling Coefficient (e Å), Anharmonicities (e V), and $\beta(0)$ for CAR(j), $j = 2, ..., 25$

n	$\mu+,+$	$\mu+,-$	$\mu-,-$	V+,++	V+,+−	V+,−+	V+,−−	V−,++	V−,+−	V−,−+	V−,−−	β_{all}	β_2	$\beta_{3,4}$	Ω_+	Ω_-	Ω_{+3}
2	−1.197	−2.525	−1.342	0.013	−2.056	1.107	0.000	−0.474	−0.146	0.145	1.135	0.97	1.00	1.00	3.09	4.84	
3	−1.333	−2.878	−1.631	0.055	−1.970	1.248	0.051	−0.361	−0.114	0.215	1.339	1.61	1.40	1.40	2.92	4.56	
4	−1.422	−3.142	−1.993	0.097	−1.817	1.304	0.015	−0.257	−0.173	0.203	1.375	2.36	2.32	2.32	2.79	4.35	
5	−1.463	−3.174	−2.412	0.138	−1.550	1.207	−0.163	−0.172	−0.352	0.026	0.922	3.16	3.24	3.24	2.69	4.20	
6	−1.459	−3.248	−1.480	0.173	−1.435	1.439	0.390	0.002	−0.258	0.522	1.408	3.96	5.47	4.02	2.62	4.10	
7	−1.420	−3.781	−2.550	0.200	−1.420	1.509	0.217	0.044	−0.022	0.457	1.979	4.72	5.38	5.38	2.56	4.01	3.89
8	−1.356	−3.949	−3.075	0.216	−1.286	1.504	0.134	0.109	−0.131	0.398	2.030	5.43	6.00	6.00	2.51	3.94	3.75
9	−1.278	−4.045	−3.448	0.224	−1.152	1.490	0.078	0.169	−0.191	0.347	2.012	6.04	6.51	6.51	2.47	3.89	3.62
10	−1.194	−4.064	−3.683	0.224	−1.018	1.457	0.034	0.220	−0.223	0.291	1.893	6.58	7.11	7.41	2.44	3.85	3.51
11	−1.109	−3.540	−3.219	0.220	−0.779	1.223	−0.054	0.222	−0.223	0.115	0.929	6.99	9.18	7.58	2.41	3.82	3.42
12	−1.027	−4.170	−3.713	0.212	−0.832	1.479	0.069	0.324	−0.143	0.282	1.872	7.40	7.22	8.04	2.39	3.82	3.33
13	−0.948	−4.298	−4.010	0.201	−0.765	1.493	0.047	0.364	−0.166	0.261	2.051	7.73	6.97	8.10	2.37	3.80	3.25
14	−0.874	−4.322	−4.046	0.189	−0.691	1.479	0.036	0.394	−0.159	0.231	2.032	8.02	6.78	8.22	2.35	3.79	3.18
15	−0.808	−4.243	−3.948	0.177	−0.611	1.429	0.018	0.409	−0.148	0.184	1.828	8.29	6.24	8.01	2.34	3.78	3.12
16	−0.746	−4.224	−3.410	0.165	−0.555	1.430	0.055	0.438	−0.085	0.195	1.723	8.48	9.60	7.13	2.32	3.78	3.06
17	−0.689	−4.396	−3.703	0.153	−0.524	1.460	0.046	0.468	−0.094	0.186	1.995	8.69	7.54	9.90	2.31	3.78	3.01
18	−0.639	−4.406	−3.623	0.141	−0.479	1.444	0.042	0.483	−0.083	0.166	1.967	8.84	7.03	9.70	2.30	3.77	2.96
19	−0.592	−4.344	−3.471	0.130	−0.432	1.403	0.034	0.486	−0.072	0.140	1.814	9.03	6.97	9.94	2.29	3.77	2.92
20	−0.549	−4.147	−2.773	0.120	−0.383	1.339	0.045	0.478	−0.030	0.120	1.432	9.15	6.87	10.15	2.28	3.77	2.88
21	−0.510	−4.442	−3.170	0.111	−0.376	1.407	0.045	0.516	−0.039	0.131	1.892	9.08	5.51	9.10	2.27	3.77	2.84
22	−0.476	−4.450	−3.095	0.102	−0.347	1.390	0.043	0.522	−0.033	0.119	1.876	9.12	4.95	8.84	2.27	3.76	2.81
23	−0.443	−4.400	−2.999	0.094	−0.318	1.355	0.038	0.519	−0.028	0.104	1.773	9.16	4.08	9.71	2.26	3.76	2.78
24	−0.414	−4.202	−2.275	0.087	−0.283	1.291	0.041	0.504	−0.004	0.087	1.354	9.21	4.52	9.38	2.25	3.76	2.75
25	−0.387	−4.473	−2.676	0.080	−0.280	1.348	0.042	0.534	−0.010	0.095	1.790	9.23	5.26	9.91	2.25	3.76	2.72

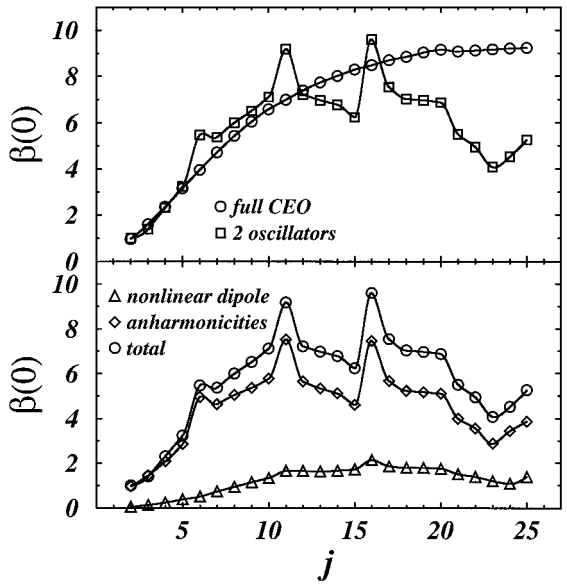

Figure 4. Variation of $\beta(0)$ (e Å^3 V^{-2}) with the number of double bonds.

in the bottom scheme of Figure 1). In each panel, the bottom left corner shows the donor, the middle square is the bridge, and the top right square shows the acceptor.

The ground-state density matrix is similar for all of these carotenoids. It is pretty much localized and shows no long-range coherence. We next turn to a closer look at the dominant electronic modes. When $\xi_{mn} \approx \xi_{nm}$, we have the creation of a bond between the mth and the nth atoms without charge transfer. When $\xi_{mn} > \xi_{nm}$, a photoinduced electron transfer occurs from the mth to the nth atom. The ξ_+ mode is primarily localized on the bridge. The interactions between the acceptor/donor and the bridge decrease as its length grows (visible in the right, left top, and bottom middle rectangles of each panel). ξ_+ for CAR(25) shows that the interaction between electrons along the bridge has a characteristic size of 15 atoms. This limit appears in CAR(7). The ξ_- oscillator has a similar shape but is more delocalized. It shows a displacement of electrons from the donor to the bridge for short bridges and from the middle of the bridge to the acceptor and its vicinity for longer bridges.

Figure 6 displays the variation of the frequencies of the oscillators ξ_+, ξ_-, and ξ_{+3} with the number of double bonds. They are noted Ω_+, Ω_-, and Ω_{+3} (ξ_{+3} is an oscillator defined below). One can note the red shift of the chromophore with increasing the number of double bonds. Ω_{+3} is not displayed below seven double bonds; the third harmonic is yet not established because the bridge is not sufficiently long to support this mode, so $\xi+_3$ cannot yet be clearly identified.

The two-oscillator model shows the opposing effect of the ξ_+ and ξ_- oscillators. With a better understanding of the relationship between molecular structure and CEO, it should be possible to minimize the involvement of the ξ_- oscillator in $\beta(0)$. Symmetry properties of the oscillator may be used to that end, and the magnitude of $\beta(0)$ could then be enhanced by up to 30% for the present system.

IV. Limitations and Extensions of the Two-Oscillator Model

Figure 4 clearly shows the range of applicability of the two-oscillator model. When the bridge length exceeds 10 double bonds, the computed $\beta(0)$ deviates from the full CEO calculation which includes all oscillators. Figure 2 shows that for CAR(25) a third mode becomes relevant. The top row of Figure 7 depicts the three oscillators involved for the longest bridge. The new oscillator (denoted ξ_{+3}) appears like the third harmonic of ξ_+.

The variation of the oscillator parameters and of $\beta(0)$ with j shown in Figures 3 and 4 is nonmonotonic and shows an interesting fine structure. For example, $\beta(0)$ and the anharmonicities have maxima for CAR(11) and CAR(16). This is due to a splitting of the ξ_- mode at a specific bridge length. The precise origin of this behavior requires a further study. However, it does not affect the global trends of $\beta(0)$, and an intuitive picture of the evolution of this hyperpolarizability may be developed without taking these effects into account. Ignoring the splitting of the ξ_- mode results in a more smooth variation of $\beta(0)$ with bridge length. This detailed structure originates from the behavior of the electrons in the polyenic bridge and is virtually independent of the ends. We thus expect it to be only

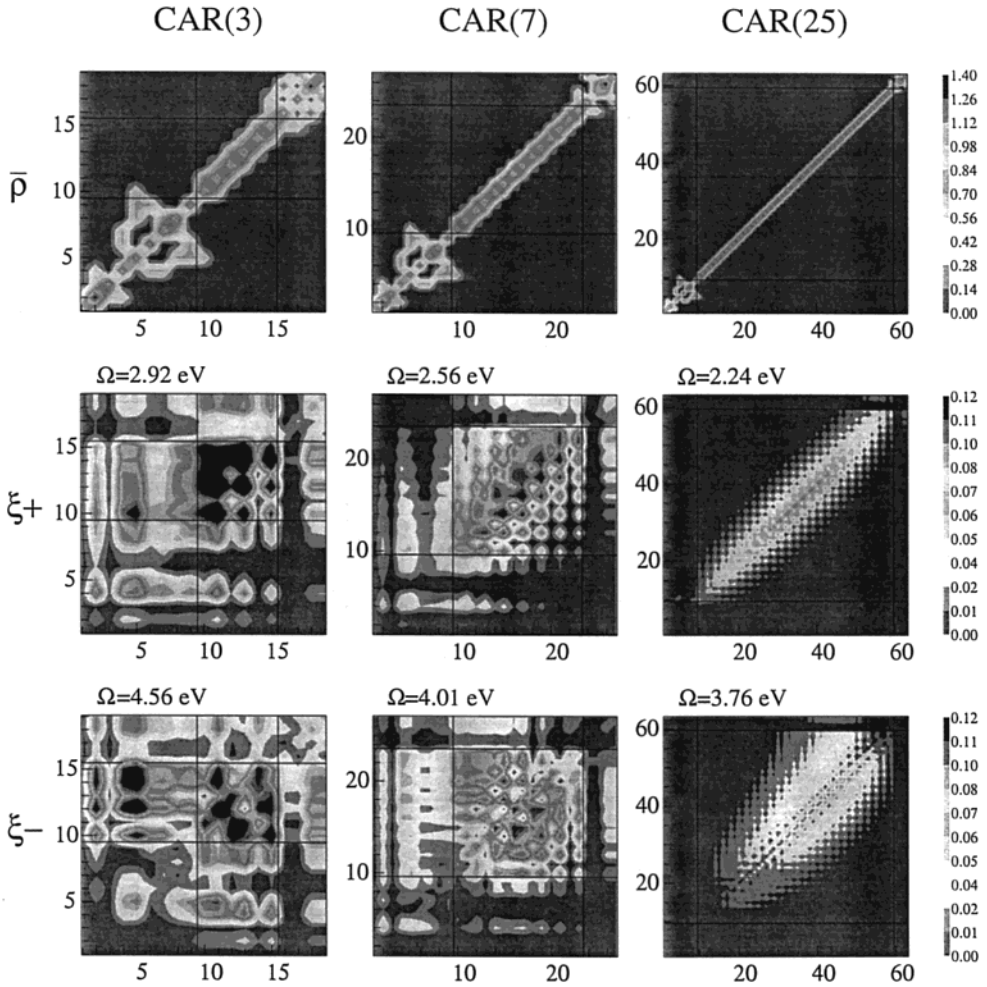

Figure 5. Density matrix for the ground state and the two dominant modes for $\beta(0)$. Top row, $\bar{\rho}$; middle row, ξ_+; bottom row, ξ_-. Left, middle, and right column: CAR(3), CAR(7), and CAR(25).

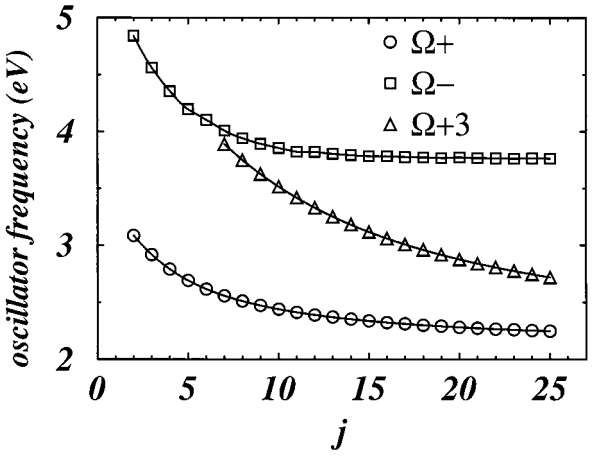

Figure 6. Variation of the frequencies (eV) of ξ_+, ξ_-, and ξ_{+3} with the number of double bonds.

weakly affected by the donor and the acceptor. A further study of the unsubsituted polyenic bridge will be desirable in order to develop a more accurate, and perhaps simpler, model of the origin of nonlinearities in such chromophores. The action of the push−pull groups could then be treated as a small perturbation of the parameters. $\beta(0)$ computed with these three oscillators (or four when ξ_- is splitted) is shown in Figure 8. Because of molecular stability problems, chromophores used in molecular engineering for nonlinear optics rarely contain more than 10 double bonds; the ξ_{+3} oscillator can be safely neglected for most NLO applications, and the splitting of the ξ_- mode can be ignored in the intuitive picture developed here.

In Figure 5 we display

$$\xi_{mn} = \sqrt{\sum_{\{\upsilon,w\}} \xi^2_{mn,\upsilon w}} \tag{18}$$

which provide a representation of the density matrix in the atomic basis set. For a better visualization of the matrix, a smoothing is done. The simple picture in the atomic representation was obtained at the expense of losing the sign of the various contributions. To show the sign of $\xi_{mn,\upsilon w}$, we need to represent explicitly the various orbitals s of each atom, because a direct summation of the contribution of all of the orbitals of each atom is not physically meaningful. A more detailed representation of $\bar{\rho}$ and the modes ξ displayed in Figure 5 can be obtained as follows. Starting with the INDO/S basis, each element of this basis can be written as $\xi_{mn,\upsilon w}$, where υ and w are respectively the orbitals of the heavy atoms m and n (s, p_x, p_y, and p_z). The hydrogen atoms are not shown. Figure 9 displays the resulting density matrices. Both axes first display orbitals s from atoms 1 to n and then orbitals p_x with the atoms in the same order, p_y and finally p_z. Each mode is now a $4n \times 4n$ rather than the $n \times n$ matrix of Figure 5. This representation retains the sign of the elements. However, we first examine the absolute values

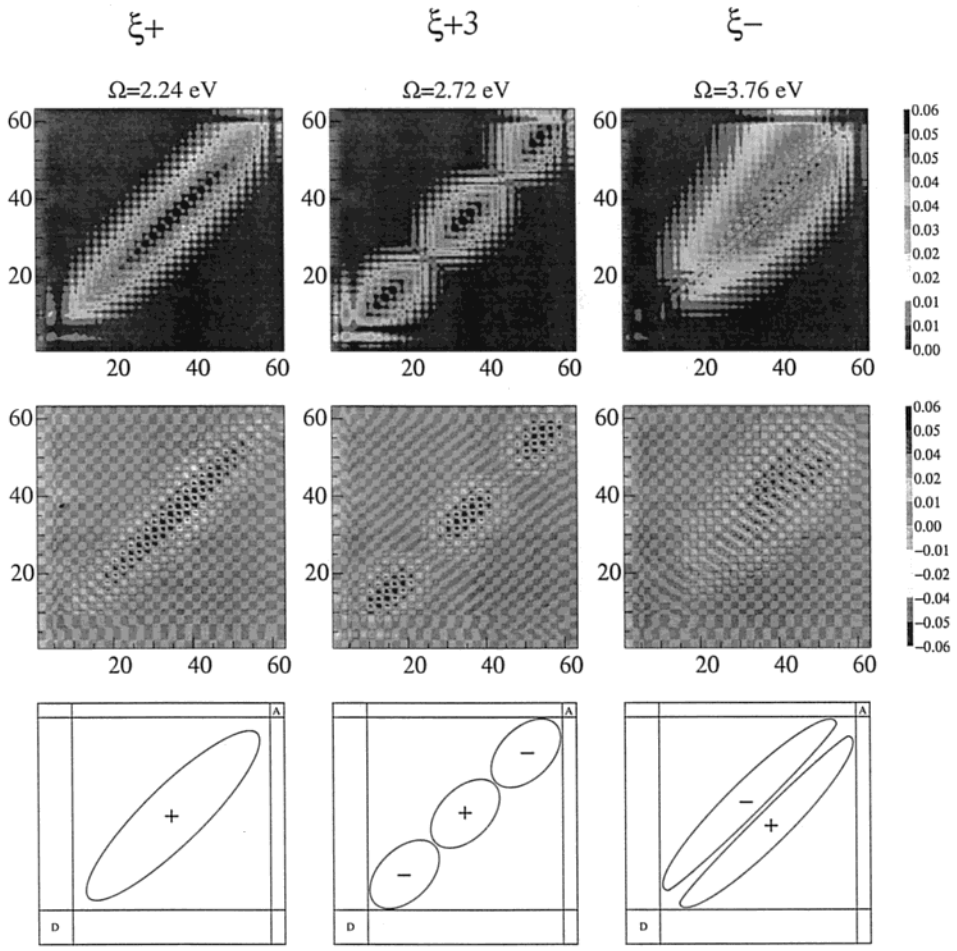

Figure 7. ξ_+, ξ_{+3}, and ξ_- oscillators of CAR(25). Upper row, ξ_{mn} in the atomic basis set; middle row, $\xi_{mn,PzPz}$; bottom row, illustration of symmetry properties.

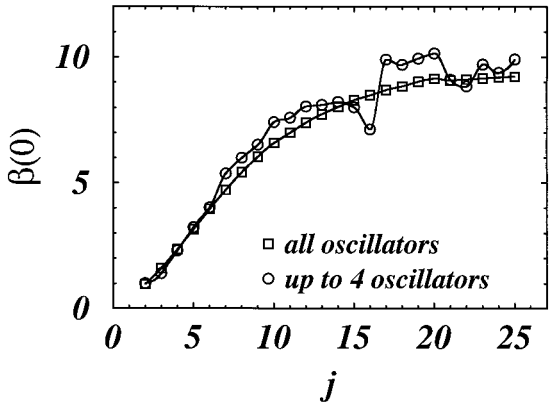

Figure 8. Variation of $\beta(0)$ computed with an extended number of oscillators with bridge length. ($\beta(0)$: e Å^3 V^{-2}).

on a logarithmic scale in order to identify the non relevant parts of the modes which can be ignored.

We can verify using Figure 9 that the σ system made by the orbitals {s, p_x, p_y} and the π system made by the orbitals p_z are decoupled in $\bar{\rho}$ as implied by the Hartree−Fock Hamiltonian (the weak coupling near the dimethyl group is due to its nonplanarity). Only the π system, formed by the p_z orbitals of all of the non-hydrogen atoms, is involved in the modes. Hereafter we only represent the relevant part (p_z, p_z) of the density matrix, neglecting the other elements, and also show the sign of the elements. The new representation is compared with the previous atomic representation in Figure 7. The atomic representation removes all of the nodes of the ξ modes. These nodes show a highly nontrivial and interesting behavior of the electrons along the bridge. The atomic representation allows a quick visualization of which parts of the molecule are involved in the mode, but the orbital representation provides additional most valuable information. The ξ_+ mode has two symmetry axes. The three parts of the mode ξ_{+3} are symmetric with respect to the diagonal elements but are antisymmetric toward each other. The ξ_- mode is antisymmetric with respect to the population elements axis. It is a *correlation mode*, in which only the bonds are involved and the mean positions of the electrons are unchanged. The symmetry properties are sketched schematically at the bottom row of Figure 7. This picture closely resembles the electromagnetic modes in cavities. A good understanding of these modes could be most useful for a description of electronic motions in polyenic bridges and for predicting the effects of push−pull groups.

Figure 10 displays the variation of the diagonal elements (populations) with atom number for CAR(7) and CAR(25). The trace of $\bar{\rho}$ is equal to the number of electrons on the external shell, and the trace of the ξ matrix vanishes. These properties are not apparent in the figure because the hydrogen atoms are not displayed. Atoms 1−9 are the donor group, followed by the polyenic bridge, and the last four atoms are the acceptor. (The atom numbers are given in Figure 1.) The top panel shows the electronic charge of the p_z orbitals of the heavy atoms. The envelope of ξ_+ and its third harmonic ξ_{+3} is clearly shown. The antisymmetry along the diagonal axis of the mode ξ_- should

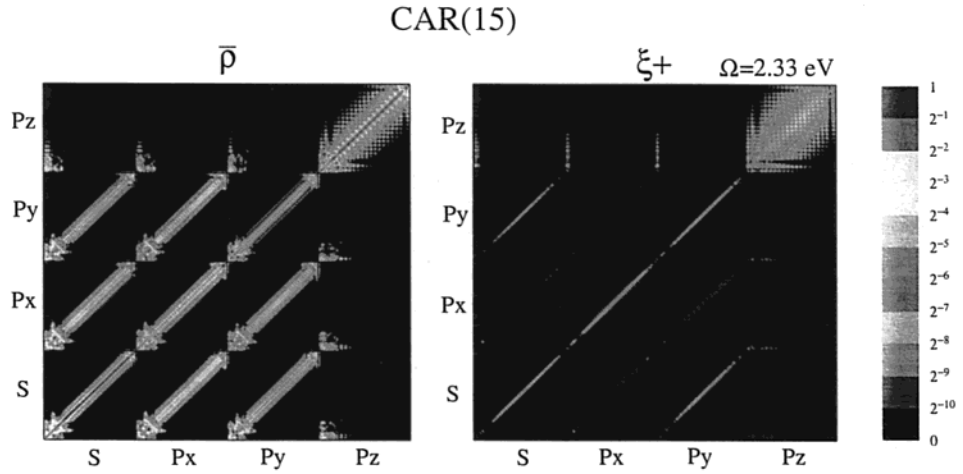

Figure 9. Representation of $\bar{\rho}$ and ξ_+ for CAR(15) in the orbital basis set.

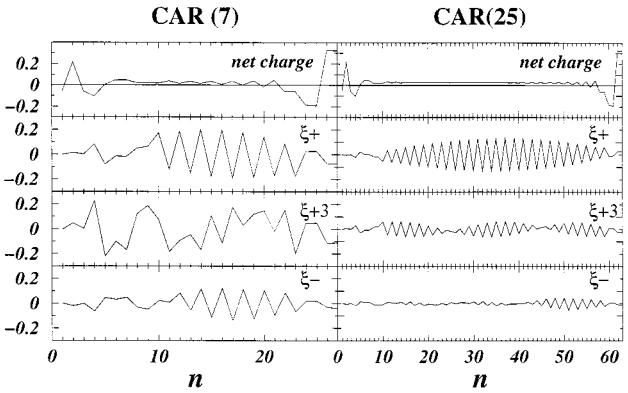

Figure 10. Diagonal elements (ξ_{mm}) of the density matrixes $\bar{\rho}$, ξ_+, ξ_{+3}, ξ_-, for CAR(7) (left column) and CAR(25) (right column).

give a zero value to all diagonal elements. This is pretty much the case in the left part of the bridge. However the right part is modulated by the acceptor. Nevertheless the amplitude remains very weak. The bottom three panels reveal the role of charge transfer in the nonlinear response.

Calculations performed on longer molecules (up to 40 double bonds) show that the present picture remains valid. As the bridge length grows, the number of anharmonic couplings that make a significant contribution to the response decreases, further simplifying the physical picture of the nonlinear response.

V. Discussion

The generic push−pull carotenoid system studied in this article clearly shows that the first optical hyperpolarizability can be described using a small number of oscillators: two oscillators are enough for chromophores commonly used in NLO engineering. For longer molecules, an additional oscillator should be included. The oscillatory behavior with j does not prevent an intuitive CEO picture.

The most important advantage of the present picture is that it provides a link between the first phenomenological description of optical nonlinearities made by Bloembergen and a rigorous theoretical approach based on a full quantum chemistry calculation. The present work establishes a firm basis and extends the early empirical descriptions of nonlinear processes, and the dynamic CEO picture is more intuitive than the static eigenstate representation. The equation of motion of the oscillators is classical. The unphysical scalings are removed, and the number of oscillators involved in the calculation of the response remains finite as the molecular size is increased. Moreover, the real-space representation of the eigenmodes allows an easy and highly intuitive understanding of the regions involved. It can be useful for manipulating the properties of the chromophore (symmetry or other) in order to remove or enhance a mode.

The CEO representation is a highly nonlinear transformation of the eigenstate representation of the optical response. Each oscillator represents a manifold of transitions involving multiple electron−hole pairs. It is therefore not possible to draw a one-to-one correspondence between the few-oscillator model and the popular scheme where the sum over states expressions is truncated to include only a few dominant states. Generally the dominant-state approach cannot be justified for off-resonant response where many states contribute. However, the few-oscillator picture works very well. The absence of a simple connection is the reason we need a new language. If there was such a connection, a new language would not be necessary. At the single excitation level, one can assign each oscillator with one state. However, the CEO also includes (approximately) infinite harmonic ladders of these state.

An improved picture may be possible in which the well-known properties (e.g., boundary conditions of the modes or coupling parameters) of the electrons in the bridge are perturbed by the donor and acceptor groups. Such a study might reveal deeper properties of the molecules which appear here as the quasiperiodic splitting of the ξ_- mode or the nodes and the symmetry properties of modes.

This study of $\beta(0)$ may be extended to higher nonlinearities such as $\gamma(0)$. This second hyperpolarizability is very important for nonlinear optics, and a similar oscillator picture could be useful for the investigation of centrosymmetric molecules with strong cubic polarizabilities.

Acknowledgment. T.T. was supported by the Ecole Normale Supérieure de Cachan in France. The support of the National Science Foundation and the Petroleum Research Fund administered by the American Chemical Society is gratefully acknowledged. Dr. Matteo Tommasini is thanked for his help all along this work.

Appendix A: The CEO Equations

We consider a system described by the following general molecular electronic Hamiltonian:[62]

$$\hat{H} = \sum_{mn\sigma} t_{mn} c^{+}_{m\sigma} c_{n\sigma} + \sum_{mnkl\sigma\sigma'} \langle nm|kl\rangle c^{+}_{m\sigma} c^{+}_{n\sigma'} c_{k\sigma'} c_{l\sigma} - \epsilon(t) \sum_{mn\sigma} \boldsymbol{\mu}_{mn} c^{+}_{m\sigma} c_{n\sigma'} \quad \text{(A1)}$$

and

$$t_{nm} = \int \chi^{*}_{n}(1) \left(\nabla_1^{\,2} - \sum_A \frac{Z_A}{|\mathbf{r}_1 - \mathbf{R}_A|} \right) \chi_m(1)\, d\mathbf{r}_1 \quad \text{(A2)}$$

$$\langle ij|kl\rangle = \int \frac{\chi^{*}_i(1)\chi^{*}_j(2)\chi_k(1)\chi_l(2)}{|\mathbf{r}_1 - \mathbf{r}_2|}\, d\mathbf{r}_1\, d\mathbf{r}_2 \quad \text{(A3)}$$

t is the core-Hamiltonian describing the kinetic energy and nuclear attraction of an electron, and $\langle ij|kl\rangle$ describe the electromagnetical interactions between the electrons.

Here c^{+}_n and c_m are respectively the Fermi creation and annihilation operators with anticommutation relations

$$\{c_i, c^{+}_j\} = \delta_{i,j}; \quad \{c_i, c_j\} = 0 \text{ where } \{a,b\} = ab + ba \quad \text{(A4)}$$

The ground-state Hartree−Fock density matrix $\bar{\rho}$ satisfies

$$[F(\bar{\rho}), \bar{\rho}] = 0 \quad \text{(A5)}$$

where the Fock operator is

$$F(\bar{\rho}) = t + V(\bar{\rho}) \quad \text{(A6)}$$

with

$$\hat{V} = \hat{J} - \hat{K} \quad \text{(A7)}$$

$$(J\bar{\rho})_{ij} = (ij|kl)\bar{\rho}_{kl} \quad \text{(A8)}$$

$$(K\bar{\rho})_{ij} = (ik|jl)\bar{\rho}_{kl} \quad \text{(A9)}$$

$\hat{J}$ is the Coulomb operator, and $\hat{K}$ is the exchange operator.

When the molecule interacts with a time-dependent electromagnetic field, its density matrix becomes time-dependent as well and can be written as

$$\rho(t) = \bar{\rho} + \delta\rho(t) \quad \text{(A10)}$$

Separating the hole−particle (ξ) and particle−particle/hole−hole ($T(\xi)$) contributions, we obtain eq 5. Using eqs 5 and 6, we have

$$\xi = [[\xi, \bar{\rho}], \bar{\rho}] \quad \text{(A11)}$$

$T(\xi(t))$ can be expressed in terms of $\xi(t)$ (eq 7). For computing the second-order response, it is sufficient to adopt the following approximation:

$$T(\xi) \approx \frac{1}{2}[[\xi, \bar{\rho}], \xi] \quad \text{(A12)}$$

The time dependent Hartree−Fock equations of the density matrix are

$$i\frac{\partial \rho(t)}{\partial t} = i\frac{\partial \delta\rho(t)}{\partial t} = [F(\rho), \rho] - \epsilon(t)\cdot[\boldsymbol{\mu}, \rho] \quad \text{(A13)}$$

Projecting into the particle−hole subspace, we obtain the following equation of motion:

$$i\frac{\partial \xi}{\partial t} - L\xi = R(\xi)_{p-h} - \epsilon(t)\cdot[\boldsymbol{\mu}, \bar{\rho}] \quad \text{(A14)}$$

where L is a *superoperator* in the Liouville−von Neumann space given by

$$L\xi = [F(\bar{\rho}), \xi] + [V(\xi), \bar{\rho}] \quad \text{(A15)}$$

and

$$R(\xi) = [F(\xi), \xi + T(\xi)] + [F(T(\xi)), \bar{\rho} + \xi] - \epsilon[\boldsymbol{\mu}, \xi + T(\xi)] \quad \text{(A16)}$$

is the nonlinear part of the equation.

The time dependent polarization responsible for all of the optical properties of the molecule is given by

$$P(t) = Tr(\boldsymbol{\mu}\delta\rho(t)) = Tr\{\boldsymbol{\mu}[\xi(t) + T(\xi(t))]\} \quad \text{(A17)}$$

Ω_α are the eigenvalues of eq 8, and we have the relations $\xi_{-\alpha} = \xi^{+}_{\alpha}$ and $z_{-\alpha} = z^{*}_{-\alpha}$. The oscillator variables are the eigenmodes of the linear part of eq 12, and they satisfy eq 8. Combining eqs 10 and A14, we find that z_α satisfies (12) with

$$\boldsymbol{\mu}_\alpha = Tr([\bar{\rho}, \xi_{-\alpha}][\boldsymbol{\mu}, \bar{\rho}]) \quad \text{(A18)}$$

$$\boldsymbol{\mu}_{\alpha,\beta} = Tr([\bar{\rho}, \xi_{-\alpha}][\boldsymbol{\mu}, \xi_\beta]) \quad \text{(A19)}$$

$$V_{\alpha,\beta\gamma} = Tr\left\{[\bar{\rho}, \xi_{-\alpha}]\left([V(\xi_\beta), \xi_\gamma] + \left[V\left(\frac{1}{2}[[\xi_\beta, \bar{\rho}], \xi_\gamma]\right), \bar{\rho}\right]\right)\right\} \quad \text{(A20)}$$

We next expand z in powers of the external field:

$$z = z^{(1)} + z^{(2)} + z^{(3)} + \ldots \quad \text{(A21)}$$

We further define

$$\tilde{\boldsymbol{\mu}}_{\boldsymbol{\beta}} \equiv Tr(\boldsymbol{\mu}\xi_\beta); \; \tilde{\boldsymbol{\mu}}_{\beta\gamma} \equiv \frac{1}{2}Tr(\boldsymbol{\mu}[[\xi_\beta, \bar{\rho}], \xi_\gamma]) \quad \text{(A22)}$$

For the static second-order response, eq 12 assumes the form

$$\Omega_\alpha z_\alpha = \epsilon\cdot\boldsymbol{\mu}_\alpha + \epsilon\cdot\sum_\beta \boldsymbol{\mu}_{\alpha,\beta} z_\beta - \sum_{\beta\gamma} V_{\alpha,\beta\gamma} z_\beta z_\gamma \quad \text{(A23)}$$

The matrices $\bar{\rho}$, $\boldsymbol{\mu}$, and ξ_α are real, and V is a real tetradic operator. They satisfy

$$\boldsymbol{\mu}_\alpha = \boldsymbol{\mu}_{-\alpha} = \tilde{\boldsymbol{\mu}}_\alpha \quad \text{and } \tilde{\boldsymbol{\mu}}_{-\alpha\beta} = \frac{1}{2}\boldsymbol{\mu}_{\alpha,\beta} \quad \text{(A24)}$$

Appendix B: Computation of Polarizabilities

The TDHF equations may be solved by expanding the density matrix in power of the external field:

$$\xi = \xi^{(1)} + \xi^{(2)} + \ldots \quad \text{and } T(\xi) = T^{(2)}(\xi) + T^{(3)}(\xi) + \ldots \quad \text{(B1)}$$

where $T^{(j)}(\xi)$ may be expressed in terms of $\xi^{(j)}$ using eq 12. We thus obtain for the jth order polarization

$$P^{(j)}(t) = Tr(\boldsymbol{\mu}\delta\rho^{(j)}) \quad \text{(B2)}$$

where

$$\delta\rho^{(j)}(t) = \xi^{(j)}(t) + T^{(j)}(\xi(t)) \quad \text{(B3)}$$

and

$$T^{(1)}(t) = 0 \quad \text{and } T^{(2)}(t) = (I - 2\bar{\rho})\cdot(\xi^{(1)}(t))^2 \quad \text{(B4)}$$

We need to solve the following linear inhomogeneous equation:

$$i\frac{\partial \xi^{(j)}(t)}{\partial t} - L\xi^{(j)}(t) = \eta^{(j)}(t) \tag{B5}$$

where $\eta^{(j)}(t)$ are

$$\eta^{(1)}(t) = -\epsilon(t)[\boldsymbol{\mu},\bar{\rho}] \tag{B6}$$

and

$$\eta^{(2)}(t) = [[([V(\delta\rho^{(1)}(t)),\delta\rho^{(1)}(t)] + [V(T^{(2)}(t)),\bar{\rho}] - \epsilon(t)[\boldsymbol{\mu},\delta\rho^{(1)}(t)]),\bar{\rho}],\bar{\rho}] \tag{B7}$$

It can be shown that the density matrix may be expanded as eq 10 with eq 7. In this expansion, α is an oscillator described by the two operators ξ_α and $\xi_\alpha{}^+$. These operators are related to the oscillator coordinates and the momenta by eq 11.

Equation 13 for the two lowest order static polarizations gives expressions 14 and 16. From eq A23, we have for $\alpha > 0$

$$z_\alpha^{(1)} = \frac{\boldsymbol{\mu}_\alpha}{\Omega_\alpha} \tag{B8}$$

and

$$z_\alpha^{(2)} = -\sum_{\beta,\gamma} U_{\alpha,\beta\gamma}\frac{\boldsymbol{\mu}_\beta\boldsymbol{\mu}_\gamma}{\Omega_\alpha\Omega_\beta\Omega_\gamma} + \sum_\beta \frac{(\boldsymbol{\mu}_{\alpha\beta} + \boldsymbol{\mu}_{\alpha-\beta})\boldsymbol{\mu}_\beta}{\Omega_\alpha\Omega_\beta} \tag{B9}$$

Equation 15 for the off-resonant $\alpha(0) \equiv \alpha(0;0)$ is obtained by substituting eq B8 in eq 14. Substituting eqs B8 and B9 into eq 16, results in eq 17 for $\beta(0) \equiv \beta(0;0,0)$.

Here

$$U_{\alpha,\beta\gamma} \equiv V_{\alpha,\beta\gamma} + V_{\alpha,\beta-\gamma} + V_{\alpha,-\beta\gamma} + V_{\alpha,-\beta-\gamma} \tag{B10}$$

and

$$\bar{\boldsymbol{\mu}}_{\beta,\gamma} \equiv \tilde{\boldsymbol{\mu}}_{\beta\gamma} + \tilde{\boldsymbol{\mu}}_{\beta-\gamma} + \tilde{\boldsymbol{\mu}}_{-\beta\gamma} + \tilde{\boldsymbol{\mu}}_{-\beta-\gamma} \tag{B11}$$

Appendix C: Units

To get a convenient order of magnitude for the quantities computed, we used the following units basis: {e, V, Å}. Here are the relationships with other units:

(1) First hyperpolarizability:

$\beta(0)$ and its contributions are displayed in e Å ^{3} V^{-2}.

1.0 e Å^3 V^{-2} ↔ 43.2 × 10^{-30} esu and 1.0 × 10^{-30} esu ↔ 2.31 × 10^{-2} e Å^3 V^{-2}.

(2) Dipole moment:

Dipole moments are displayed in e Å.

1.0 e Å ↔ 4.81 D and 1.0 D ↔ 2.08 × 10^{-1} e Å.

1.0 e Å ↔ 4.81 × 10^{-18} esu cm and 1.0 × 10^{-18} esu cm ↔ 2.08 × 10^{-1}e Å.

(3) Energies and frequencies are in eV.

(4) The charge is displayed in units of the electron charge, e.

References and Notes

(1) Chemla, D. S.; Zyss, J. *Nonlinear Optical Properties of Organic Molecules and Cristal*; Chemla, D. S., Zyss, J., Eds.; Academic Press: Orlando, 1987; Vol. 1. For a historical account, see also: Kajzar, F.; Zyss, J. *Nonlinear Opt.* **1995**, *9*, 3.

(2) Molecular Nonlinear Optics: Materials, Phenomena and Devices. Dick, B., Stegeman, G., Twiegand, R., Zyss, J., Eds.; *Chem. Phys.* **1999**, *245* (1−3), 1−544.

(3) *Nonlinear Optics of Organic Molecules and Polymers*; Nalwa, H. S., Miyata, S., Eds.; CRC Press: Boca Raton, FL, 1997.

(4) Zyss, J. *J. Chem. Phys*. **1993**, *98*, 6583.

(5) Zyss, J.; Ledoux, I. *Chem. Rev. 1994*, *94*, 77−105.

(6) Dhenaut, C.; Ledoux, I.; Samuel, I. D. W.; Zyss, J.; Bourgault, M.; Le Bozec, H. *Nature* **1995**, *374*, 339.

(7) Zyss, J. to be published

(8) Mukamel, S.; Tretiak, S.; Wagersreiter, T.; Chernyak, V. *Science* **1977**, 277. Mukamel, S.; Takahashi, A.; Wang H. X.; Chen, G. *Science*, **1994**, *266*, 250.

(9) Takahashi, A.; Mukamek, S. *J. Chem. Phys*. **1994**, *100*, 2399.

(10) Mukamel, S.; Wang, H. X. *Phys. Rev. Lett.* **1992**, *69*, 65.

(11) Bloembergen, N. *Nonlinear Optics*; Benjamin: New York, 1965.

(12) Rosenfeld, L. *Theory of electrons*; Dover: New York, 1952.

(13) Chemla, D. S. *Phys. Rev. Lett*. **1971**, *26*, 1441.

(14) Choy, M.; Ciraci, S.; Byer, R. L. *IEEE J. Quantum Electron*. **1975**, *11* (Vol. QE), 40.

(15) Lalamam, S. J.; Garito, A. F. *Phys. Rev. A* **1979**, *20*, 1179.

(16) Docherty, V. J.; Pugh, D.; Morley, J. *J. Chem. Soc., Faraday Trans. 2* **1985**, *81*, 1179.

(17) Kanis, D. R.; Ratner, M. A.; Marks, T. J.; Zerner, M. C. *Chem. Mater*. **1991**, *3*, 19.

(18) Ward, J. F. *Rev. Mod. Phys*. **1965**, *37*, 1.

(19) Dirk, C. W.; Kuzyk, M. G. *Phys. Rev. A* **1989**, *39*, 1219.

(20) Kuzyk, M. G.; Dirk, C. W. *Phys. Rev. A* **1990**, *41*, 5098.

(21) Mulliken, R. S. *J. Am. Chem. Soc*. **1952**, *74*, 811.

(22) Murrel, J. N. *J. Am. Chem. Soc*. **1959**, *81*, 5037.

(23) Oudar, J. L. *J. Chem. Phys*. **1977**, *67*, 446.

(24) Blanchard-Desce, M.; Barzoukas, M. *J. Opt. Soc. Am. B* **1998**, *302*.

(25) Wortmann, R.; Kramer, P.; Glania, C.; Lebus, S.; Detzer, N. *Chem. Phys*. **1993**, *99*, 173.

(26) Marder, S. R.; Berattan, D. N.; Cheng, L. T. *Science* **1991**, *252*, 103.

(27) Toussaere, E.; Zyss, J. *Thin Solid Films* **1993**, *234*, 432; 454.

(28) Bosshard, C.; Knöpfle, G.; Prêtre, P.; Günter, P. *J. Appl. Phys*. **1992**, *71*, 1594.

(29) Guggenheim, E. A. *Trans. Faraday Soc*. **1949**, *45*, 714.

(30) Minkin, V. I.; Osipov, O. A.; Zhdanov, Yu. A. *Dipole Moments in Organic Chemistry in Physical Methods in Organic Chemistry series*; Plenum: New York, 1970.

(31) McClellan, A. L. *Table of experimental dipole moments*; Freeman: San Francisco, CA, 1963.

(32) Liptay, W. In *Excited States*; Lim, E. C., Ed.; Academic Press: New York, 1974; Vol.1, p 129 .

(33) Wortmann, R.; Glania, C.; Krämer, P.; Lukaszuk, K.; Matschiner, R.; Twieg, R. J.; You, F. *Chem. Phys*. **2000**, 245, 107.

(34) Levine, B. F.; Bethea, C. *J. Chem. Phys*. **1975**, *65*, 2429. Oudar, J. L.; Chemla, D. S. *J. Chem. Phys*. **1977**, *66*, 2664.

(35) Singer, K. D.; Garito, A. F. *J. Chem. Phys*. **1987**, *75*, 3572.

(36) Ledoux, I.; Zyss, J. *Chem. Phys*. **1982**, *73*, 203.

(37) Terhune, R. W.; Maker, P. D.; Savage, C. M. *Phys. Rev. Lett*. **1965**, *14*, 681.

(38) Maker, P. D. *Phys. Rev. A* **1970**, *1*, 923.

(39) Clays, K.; Persoons, A. *Phys. Rev. Lett*. **1991**, *66*, 2980.

(40) Ledoux, I. Zyss, J. *Chem. Rev*. **1994**, *94*, 77−105.

(41) Brasselet, S.; Zyss, J. *J. Opt. Soc. Am. B* **1998**, *15(1)*, 257.

(42) Meshulam, G.; Berkovic, G.; Kotler, Z.; Ben-Asuly, A.; Mazor, R.; Shapiro L.; Khodorkovski, V. *Proceedings 5th International Conference on Organic Nonlinear Optics*; Davos, Switzerland, March 12th−16th 2000; Poster E−13.

(43) Toussaere, E. Ph.D. Thesis, Université Orsay−Paris XI, 1993

(44) Heflin, R.; Wong, K. Y.; Zamani-Kamiri, O.; Garito, A. F. *Phys. Rev. B* **1988**, *38*, 1573.

(45) Bubeck, C. Nonlinear Optical Properties of Oligomers. In *Electronic Materials−The Oligomer Approach*; Wegner, G., Müllen, K., Eds.; VCH: Weinheim, Germany, 1998; Chapter 8, pp 449−478.

(46) Joffre, M.; Yaron, D.; Silbey, R.; Zyss, J. *J. Chem. Phys*. **1992**, *97*, 5607.

(47) Pierce, P. B.; Zyss, J.; Joffre, M. *Proc. SPIE* **1993**, *2025*, 13.

(48) Brasselet, S.; Zyss, J. *Int. J. Nonlin. Opt. Phys. Mater*. **1996**, *5*, 671.

(49) Cho, M.; Kim, H. S.; Jeon, S.-J. *J. Chem. Phys*. **1998**, *108*, 7114.

(50) Lee, Y,-K.; Jeon S.-J.; Cho, M. *J. Am. Chem. Soc.* **1998**, *120*, 10921.

(51) Cho, M.; Ledoux, I.; Zyss, J., et al. Submitted to *J. Chem. Phys*.

(52) Philips, J. C.; Van Vechten, J. A. *Phys. Rev. Lett*. **1969**, *22*, 705.

(53) Levine, B. F. *Phys. Rev. B* **1973**, *7*, 2600.

(54) Marder, S. R.; Berattan, D. N.; Cheng, L. T. *Science* **1991**, *252*, 103.

(55) Unsöld, A. *Z. Phys.* **1928**, *43*, 388.

(56) Robinson, F. N. H. *Bell Syst. Technol. J*. **1967**, *46*, 913.

(57) Flytzanis, C.; Ducuing, J. *Phys. Rev. Lett. A* **1968**, *26*, 315.

(58) Fkyerat, A.; Guelzim, A.; Baert, F.; Zyss, J.; Périgaud, A. *Phys. Rev. B* **1996**, *53*, 16236.

(59) Zyss, J. *J. Chem. Phys*. **1979**, *70*, 3333; 3341; *J. Chem. Phys*. **1979**, *71*, 909.

(60) Levenson, R.; Zyss, J. In *Materials for Optoelectronics*; Quillec, M., Ed.; Kluwer: Dordrecht, The Netherlands, 1996; Chapter C−III, pp 341−374.

(61) Kanis, D. R.; Ratner, M. A.; Marks, T. J. *Chem. Rev.* **1994**, *94*, 195.

(62) Szabo, A.; Ostlund, N. S. *Modern Quantum Chemistry*; Dover Publication: Mineola, NY, 1996.

(63) Tretiak, S.; Chernyak, V.; Mukamel, S. *Chem. Phys. Lett* **1996**, *259*, 55.

(64) Tretiak, S.; Chernyak, V.; Mukamel, S. *J. Chem. Phys*. **1996**, *105*, 8914.

(65) Chernyak, V.; Mukamel, S. *Chem. Phys.* **1996**, *104*, 444.

(66) Tretiak, S.; Chernyak, V.; Mukamel, S. *J. Chem. Phys*. **1996**, *105*, 8914.

(67) Meier, T.; Mukamel, S. *Phys. Rev. Lett*. **1996**, *77*, 3471.

(68) Meier, T.; Tretiak, S.; Chernyak, V.; Mukamel, S. *Phys. Rev. B* **1997**, *55*, 4960.

(69) Davidson, E. R. *Reduced Density Matrix in Quantum Chemistry*; Academic Press: New York, 1976.

(70) McWeeny, R.; Sutcliffe, B. T. *Method of Molecular Quantum Mechanics*; Academic Press: New York, 1976.

(71) Milliken, R. S. *J. Chem Phys*. **1955**, *23*, 1833.

(72) Lowdin, P. O. *Phys. Rev*. **1955**, *97*, 1474; *Adv. Phys.* **1956**, *5*, 1.

(73) Spesier, S. *Chem. Rev*. **1996**, *96*, 1953.

(74) Kanis, D. R.; Ratner, M. A.; Marks, T. J. *Chem. Rev*. **1994**, *94*, 195.

(75) Blanchard-Desce, M.; Runser, C.; Fort, A.; Barzoukas, M.; Lehn, J.-M.; Bloy, V.; Alain, V. *Chem. Phys*. **1995**, *199*, 253.

(76) Blanchard-Desce, M.; Lehn, J.-M.; Barzoukas, M.; Ledoux, I.; Zyss, J. *Chem. Phys*. **1994**, *181*, 281.

(77) Frisch, M. J.; Trucks, G. W.; Schlegel, H. B.; Scuseria, G. E.; Robb, M. A.; Cheeseman, J. R.; Zakrzewski, V. G.; Montgomery, J. A., Jr.; Stratmann, R. E.; Burant, J. C.; Dapprich, S.; Millam, J. M.; Daniels, A. D.; Kudin, K. N.; Strain, M. C.; Farkas, O.; Tomasi, J.; Barone, V.; Cossi, M.; Cammi, R.; Mennucci, B.; Pomelli, C.; Adamo, C.; Clifford, S.; Ochterski, J.; Petersson, G. A.; Ayala, P. Y.; Cui, Q.; Morokuma, K.; Malick, D. K.; Rabuck, A. D.; Raghavachari, K.; Foresman, J. B.; Cioslowski, J.; Ortiz, J. V.; Stefanov, B. B.; Liu, G.; Liashenko, A.; Piskorz, P.; Komaromi, I.; Gomperts, R.; Martin, R. L.; Fox, D. J.; Keith, T.; Al-Laham, M. A.; Peng, C. Y.; Nanayakkara, A.; Gonzalez, C.; Challacombe, M.; Gill, P. M. W.; Johnson, B. G.; Chen, W.; Wong, M. W.; Andres, J. L.; Head-Gordon, M.; Replogle, E. S.; Pople, J. A. *Gaussian 98*; Gaussian, Inc.: Pittsburgh, PA, 1998.

(78) Pople, J. A.; Beveridge, D. L.; Dobosh, P. *J. Chem. Phys*. **1967**, *47*, 2026.

(79) Ridley, J.; Zerner, M. C. *Theor. Chim. Acta* **1973**, *32*, 171.

(80) Zerner, M. C.; Loew, G. H.; Kirchner, R. F.; Mueller-Westerhoff, U. T. *J. Am. Chem. Soc*. **1980**, *102*, 589.

(81) Chernyak, V.; Schultz, M. F.; Mukamel, S.; Tretiak, S.; Tsiper, E. V. *J. Chem. Phys.* **2000**, *113*, 36.